# Untwisting Moiré Physics: Almost Ideal Bands and Fractional Chern Insulators in Periodically Strained Monolayer Graphene

Qiang Gao,[1] Junkai Dong[●],[2] Patrick Ledwith,[2] Daniel Parker,[2] and Eslam Khalaf[1]

[1]*Department of Physics, The University of Texas at Austin, Texas 78712, USA*
[2]*Department of Physics, Harvard University, Cambridge, Massachusetts 02138, USA*

Moiré systems have emerged in recent years as a rich platform to study strong correlations. Here, we will propose a simple, experimentally feasible setup based on periodically strained graphene that reproduces several key aspects of twisted moiré heterostructures—but without introducing a twist. We consider a monolayer graphene sheet subject to a $C_2$-breaking periodic strain-induced pseudomagnetic field with period $L_M \gg a$, along with a scalar potential of the same period. This system has *almost ideal* flat bands with valley-resolved Chern number $\pm 1$, where the deviation from ideal band geometry is analytically controlled and exponentially small in the dimensionless ratio $(L_M/l_B)^2$, where $l_B$ is the magnetic length corresponding to the maximum value of the pseudomagnetic field. Moreover, the scalar potential can tune the bandwidth far below the Coulomb scale, making this a very promising platform for strongly interacting topological phases. Using a combination of strong-coupling theory and self-consistent Hartree-Fock, we find quantum anomalous Hall states at integer fillings. At fractional filling, exact diagonaliztion reveals a fractional Chern insulator at parameters in the experimentally feasible range. Overall, we find that this system has larger interaction-induced gaps, smaller quasiparticle dispersion, and enhanced tunability compared to twisted graphene systems, even in their ideal limit.

*Introduction.*—The discovery of correlated states in moiré materials has transformed the study of strongly correlated phases [1–6]. Moiré materials provide a platform where the bandwidth can be tuned by adjusting the twist angle, enabling the realization of topologically trivial and nontrivial strongly interacting bands. Beyond bandwidth and topology, recent works have identified the quantum geometry of wave functions [7–12] as a central ingredient in understanding interacting physics, including the effective quasiparticle dispersion [12–15], the stability of correlated topological phases [8,9,16–19], and the properties of collective excitations [7,10,14,20–22]. However, compared to bandwidth, quantum geometry is significantly more difficult to tune since it is mostly fixed by the form of the moiré potential.

A prominent example is twisted bilayer graphene (TBG), where an ideal limit [23] can be theoretically achieved by tuning intrasublattice moiré tunneling to zero. The resulting model exhibits flat $C = \pm 1$ bands satisfying the trace condition [8,9,11,24], which relates the Fubini-study metric to the Berry curvature. These are called "ideal bands," and are equivalent to those of the lowest Landau level in a nonuniform magnetic field [8,9,25], making them a promising platform to realize [26] exotic phases such as fractional Chern insulators (FCIs) [8,9,16–19] and skyrmion superconductivity [27,28]. However, known experimental knobs cannot tune TBG to its ideal limit (although lattice

relaxation moves couplings toward this limit [29–31]). Alternating-twist multilayer generalizations [32–36] may improve the situation, particularly at higher magic angles [31], but still do not offer sufficient tunability. Other moiré systems employing Bernal-stacked bilayer graphene such as twisted monobilayer [37–43] or double bilayer [44–51] admit idealized models [52–55] but in practice involve additional terms such as trigonal warping [56] that move them even further from ideal conditions [57].

Strain engineering provides another route to realize narrow bands with strong correlations [60–64]. Strain acts on graphene as a pseudomagnetic field (PMF) with equal and opposite strength in each valley [65–74]. Early theoretical works focused on strain profiles that realize a uniform PMF to emulate Landau level physics [69,75,76]. However, these realizations require the atomic displacement $u$ to grow quadratically with distance [77], which is only possible experimentally within a limited length scale ($\sim 10$–$100$ nm) [78,79]. A more controllable setup is that of periodic strain, which yields a periodic PMF with a vanishing average over the unit cell. This is realized experimentally by suspending graphene on a network of nanorods [80], or through the spontaneous buckling of graphene on substrates such as $NbSe_2$ where a $C_2$-breaking PMF was recently observed [81]. This PMF gives rise to narrow bands [82–86], whose quantum geometry and the resulting interaction physics remain to be explored.

Reference [23] has shown that a fully flat ideal band is realized in a Dirac system if the sublattice-polarized wave functions at the Dirac point have zeros in real space [23,87]. However, in contrast to moiré potentials that give rise to a *non-Abelian* gauge field [23,88], strain only leads to an *Abelian* field. This poses a challenge for realizing ideal bands in strained graphene, since the wave functions of a Dirac particle in an Abelian field are exponential functions that can never have zeros.

In this Letter, we will show that by combining slowly varying periodic $C_2$-breaking PMF with a scalar potential of the same periodicity in monolayer graphene, we can realize an isolated *almost ideal* flat band with valley resolved Chern number $C = \pm 1$. By *almost ideal*, we means that deviations from ideality, i.e., trace condition violation, are analytically controlled and exponentially small in $\alpha \sim (L_M/l_B)^2$. Here, $L_M \gg a_{\text{graphene}}$ is the period of the PMF and $l_B$ is the magnetic length corresponding to the maximal PMF. This deviation is $\ll 1$ for experimentally realistic parameters. We note a similar setup proposed earlier combining $C_2$-*symmetric* PMF with periodic scalar field to gap out the graphene Dirac cone [71].

We show that the bandwidth is tunable via a scalar field, and can be made significantly smaller than the Coulomb scale. We study this limit of small bandwidth using analytical strong coupling theory, Hartree-Fock (HF) and exact diagonalization (ED). We provide evidence for quantum anomalous Hall (QAH) states and fractional Chern insulators (FCIs) at integer and fractional fillings, respectively. Our results suggest that this system is more tunable and has favorable parameters to realize QAH and FCI states compared to twisted graphene systems, even in their ideal limit.

*Flat bands and topology.*—Our starting point is the continuum model of strained graphene with a triangular $C_2$-breaking PMF [81] given by

$$\mathcal{B}(z, \bar{z}) = \mathcal{B}_0 \sum_{l=0}^{5} e^{i\mathbf{G}_l \cdot \mathbf{r}} = \mathcal{B}_0 \sum_{l=0}^{5} e^{\frac{i}{2}(G_l \bar{z} + \bar{G}_l z)}, \quad (1)$$

where $\mathbf{G}_l = R_{\pi l/3} \mathbf{G}_0$, $\mathbf{G}_0 = (4\pi/\sqrt{3}L_M)(1, 0)$, and $G_l \equiv G_{lx} + iG_{ly}$.

The Hamiltonian in a single valley has the form $\mathcal{H} = v_F \boldsymbol{\sigma} \cdot (-i\hbar \boldsymbol{\nabla} + e\tilde{\mathcal{A}})$ where $\boldsymbol{\nabla} \times \tilde{\mathcal{A}} = \mathcal{B}$. The other valley is generated by time-reversal symmetry $\mathcal{T}$ [89]. $\mathcal{H}$ is invariant under threefold rotations $C_3$ and $M_x \mathcal{T}$, the combination of mirror $x \mapsto -x$ and time reversal. Strain corresponding to Eq. (1) breaks both $C_2 \mathcal{T}$ and $M_y$ symmetries of graphene [82,83]. Furthermore, $\mathcal{H}$ has the chiral symmetry $\sigma_z \mathcal{H} \sigma_z = -\mathcal{H}$, which protects a single Dirac cone per valley against gapping out even though $C_2 \mathcal{T}$ symmetry is broken. A sublattice potential $\propto \sigma_z$ can be used to open a gap at the Dirac cone, but such a potential cannot be tuned in practice. Nevertheless, by noting that the sublattice polarized wave
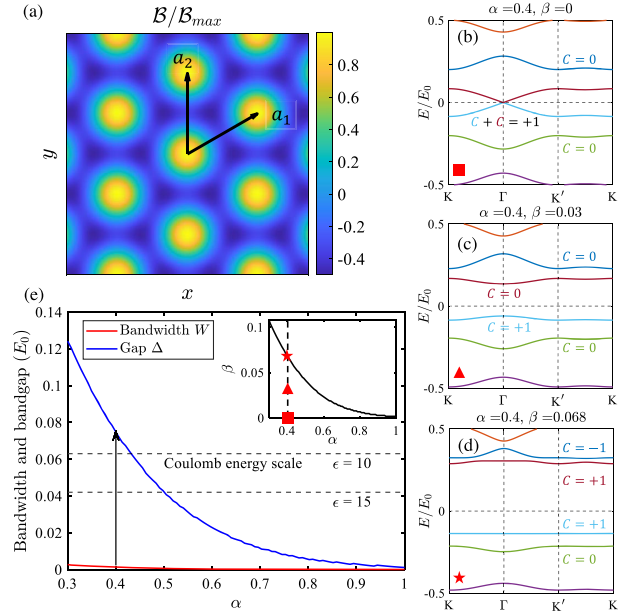


FIG. 1. (a) The PMF as described by Eq. (1). The band structures of the Hamiltonian [Eq. (2)] without (b) and with (c),(d) scalar potential. (e) The minimal bandwidth of the $C = +1$ flat band and its band gap $\Delta$ with respect to the lower band for different $\alpha$ for the value of $\beta$ that minimizes the bandwidth as shown in the inset. All energy scales are measured in units of $E_0 = \hbar v_F |G_0|$. The setup of Ref. [81] corresponds to $\alpha \approx 0.4$ and $E_0 \approx 0.3$ eV.

functions at the Dirac point are given by simple exponentials $\psi_{A/B} \propto e^{\pm \phi}$ [$-\nabla^2 \phi \propto \mathcal{B}$, see Eq. (4)], we see that a scalar potential $\propto \phi$ acts effectively as a tunable sublattice potential that gaps out the Dirac point. The explicit form of the potential is $\sigma_0 V_0 \sum_l e^{i\mathbf{G}_l \cdot \mathbf{r}}$, which matches the height buckling pattern [81] and thus is generated by applying a vertical electric field [85,90].

Let us express the Hamiltonian in dimensionless units by measuring momentum in units of $|\mathbf{G}_0| = (4\pi/\sqrt{3}L_M)$ and introducing the magnetic length for the PMF $\mathcal{B}_0 = (\hbar/el_{\mathcal{B}}^2)$, leading to

$$\mathcal{H} = E_0 \{ [\mathbf{k} + \alpha \mathcal{A}] \cdot \boldsymbol{\sigma} + \beta V(\mathbf{r}) \}. \quad (2)$$

Here, $E_0 = \hbar v_F |\mathbf{G}_0|$, $\alpha = 1/l_B^2 |\mathbf{G}_0|^2 = 3(L_M/4\pi l_B)^2$, and $\beta = V_0/E_0$. $\mathcal{A}$ and $V$ are dimensionless gauge and scalar potentials given by

$$\mathcal{A} = \sum_{l=0}^{5} e^{i\frac{\pi l}{3}} e^{\frac{i}{2}(G_l \bar{z} + \bar{G}_l z)}, \qquad V = \sum_{l=0}^{5} e^{\frac{i}{2}(G_l \bar{z} + \bar{G}_l z)}, \quad (3)$$

where $\mathcal{A} \equiv \mathcal{A}_x + i\mathcal{A}_y$. Using the experimental parameters of Ref. [81], $L_M \approx 15$ nm and $l_B \approx 3.2$ nm, we find $\alpha \approx 0.4$ and $E_0 \approx 0.3$ eV [98]. Figures 1(b) and 1(c) show band structures for $\alpha = 0.4$ without ($\beta = 0$) and with ($\beta \neq 0$) scalar potentials. For $\beta = 0$, we find a pair of isolated bands
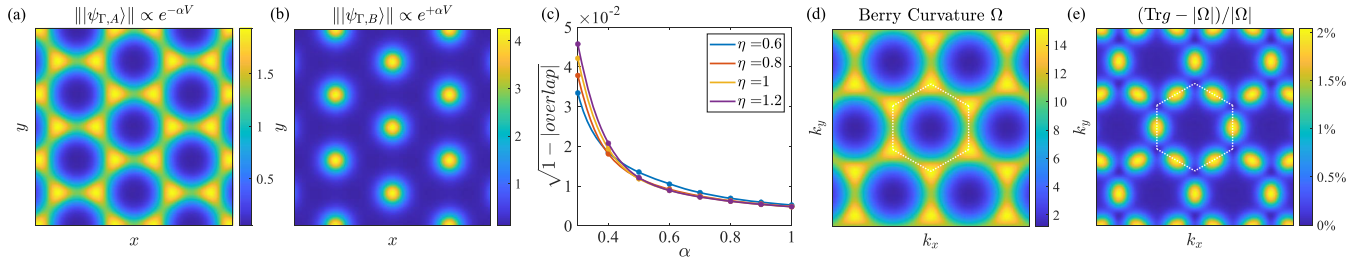
FIG. 2. (a),(b) Sublattice-polarized zero mode wave functions at the $\Gamma$ point. (c) The Brillouin-zone-averaged square root deviation $(1 - |\langle \psi_{\mathbf{k},A} | \psi_{\mathbf{k},A}^{\eta} \rangle|)^{1/2}$ between the real wave function and the ansatz in Eq. (6) for $\beta = 0$. (d),(e) The Berry curvature $\Omega$ and the trace condition violation $(\mathrm{Tr}g - |\Omega|)/|\Omega|)$ of the $C = +1$ band for $\alpha = 0.4$, $\beta = 0$. The dotted hexagons indicate the Brillouin zone.

connected by a single Dirac cone at $\Gamma$ (which corresponds to graphene $K$), protected by chiral symmetry.

To highlight the role of topology, we adopt a sublattice basis [9,92]. At $\beta = 0$, chiral symmetry implies $[\sigma_z, \mathcal{H}^2] = 0$. Thus, we can label the doubly degenerate eigenfunctions of $\mathcal{H}^2$ by a sublattice index A/B. The sublattice wave functions mix the energy eigenfunctions of $\mathcal{H}$; $\psi_{A/B,\mathbf{k}} = (1/\sqrt{2})(\psi_{\epsilon,\mathbf{k}} \pm \sigma_z \psi_{\epsilon,\mathbf{k}})$, where $\sigma_z \psi_{\epsilon,\mathbf{k}} \propto \psi_{-\epsilon,\mathbf{k}}$. Importantly, while the band wave functions around neutrality are singular at the Dirac point and cannot be assigned a Chern number, the sublattice wave functions are well-defined everywhere [9,92,93]. In the Supplemental Material (SM) [91] we show that the sum of these two Chern numbers is always odd, implying that these two bands are nontrivial within a single valley [82]. By direct computation, the sublattice $A$ ($B$) wave function has Chern number $+1$ (0) in the $K$ valley.

Adding a scalar potential with $\beta > 0$ gaps out the Dirac point and leads to an isolated $C = 1$ band polarized on sublattice A [see Fig. 1(c)]. Remarkably, the scalar potential can be tuned to obtain an almost perfectly flat band, shown in Fig. 1(d). At $\alpha = 0.4$, $\beta = 0.068$ gives the minimal bandwidth. Using a height modulation of 0.2 nm [81], this is generated by a vertical electric field of 100 mV/nm.

Figure 1(e) shows the minimal bandwidth as a function of $\alpha$ (see inset for the corresponding $\beta$ value) together with the gap to the closest band. We note that all energy scales decrease exponentially with $\alpha$. On top of this exponential squeezing, the scalar potential further flattens the topological band, leading to a minimum bandwidth that is almost 2 orders of magnitude smaller than the typical energy scale at a given $\alpha$. For interacting physics, we introduce the Coulomb scale: $V_C = e^2/(4\pi\epsilon\epsilon_0 L_M)$. In dimensionless units, $v_C = V_C/E_0 = \sqrt{3}e^2/8\pi^2\epsilon\epsilon_0 v_F \hbar \approx 0.63/\epsilon$, which is independent of $L_M$. In Fig. 1(e), we show the energy hierarchy of the bandwidth and the band gap compared to the Coulomb energy scale. The bandwidth is significantly smaller than the Coulomb scale, placing the system in the strongly interacting regime.

*Wave functions and quantum geometry.*—For $\beta = 0$, the sublattice-polarized Bloch wave functions at $\Gamma$ satisfy

$$\mathcal{D}\psi_{\Gamma,B} = 0, \qquad \mathcal{D}^{\dagger}\psi_{\Gamma,A} = 0, \qquad (4)$$

with $\mathcal{D} = -2i\partial + \alpha\bar{\mathcal{A}}$ and $\mathcal{D}^{\dagger} = -2i\bar{\partial} + \alpha\mathcal{A}$. Noting that $\mathcal{A} = -2i\bar{\partial}V$, we can solve Eq. (4) as $\psi_{\Gamma,A/B}(\mathbf{r}) = e^{\mp\alpha V(\mathbf{r})}$. These wave functions are plotted in Figs. 2(a) and 2(b), showing that the A sublattice wave function is strongly suppressed at $\mathbf{r} = 0$ and peaked at the two other $C_3$ invariant points related by $M_x\mathcal{T}$, while the B sublattice wave function is strongly peaked at $\mathbf{r} = 0$.

To understand the quantum geometry of the bands, let us review the construction of Ref. [23]. An ideal perfectly flat Chern band can be constructed for a Dirac operator if the zero mode wave function at the Dirac point $\psi_0$ has a real-space zero [99]. The ideal band wave functions take the form

$$\psi_{\mathbf{k}}(\mathbf{r}) = \frac{\sigma(z + i\tilde{B}^{-1}k)}{\sigma(z)} e^{\frac{i}{2}z\bar{k}} \psi_0(\mathbf{r}), \qquad (5)$$

where $k = k_x + ik_y$ and $\tilde{B} = (2\pi/A_{\mathrm{UC}})$ with $A_{\mathrm{UC}}$ the area of the unit cell. $\psi_{\mathbf{k}}$ satisfies $\mathcal{D}(\bar{\partial})\psi_{\mathbf{k}} = 0$ if $\mathcal{D}(\bar{\partial})\psi_0 = 0$ and transforms as a Bloch state under translations $\psi_{\mathbf{k}}(\mathbf{r} + \mathbf{R}) = e^{i\mathbf{k}\cdot\mathbf{R}}\psi_{\mathbf{k}}(\mathbf{r})$ for any lattice vector $\mathbf{R}$. The latter property follows from the properties of the modified Weierstrass sigma function [11,100].

A crucial property of the wave function [Eq. (5)] is that its cell-periodic part $u_{\mathbf{k}} = e^{-i\mathbf{k}\cdot\mathbf{r}}\psi_{\mathbf{k}}$ is holomorphic in $k$. This property is equivalent [24,101,102] to the trace condition, $\mathrm{tr}g(\mathbf{k}) = |\Omega(\mathbf{k})|$, where $g_{\mu\nu}(\mathbf{k})$ is the Fubini-study metric, defined as the symmetric part of the quantum metric tensor $\eta_{\mu\nu}(\mathbf{k}) = \langle\partial_{k_\mu}u_{\mathbf{k}}|(1 - |u_{\mathbf{k}}\rangle\langle u_{\mathbf{k}}|)|\partial_{k_\nu}u_{\mathbf{k}}\rangle$, and $\Omega(\mathbf{k})$ is the Berry curvature. Equivalently, this property has been recently interpreted as a vortex attachment condition, which enables the construction of trial FCI states that are exact ground states for repulsive short-range interactions [24,52,54]. These three equivalent properties define an ideal band.

Since the wave function $\psi_{\Gamma,A}$ is given by a simple exponential, it cannot have any zeros. However, for $\alpha$ sufficiently large [103], this wave function is exponentially small at $\mathbf{r} = 0$. As a result, we can multiply it by a regulator

$f_\eta(\mathbf{r})$ that vanishes at 0 but is close to 1 everywhere else in the unit cell; such a replacement will only change the wave function by an exponentially small term. One possible choice of regulator is $f_\eta(\mathbf{r}) = 1 - e^{\eta[V(\mathbf{r})-6]}$ for some $\mathbf{k}$-independent $\eta > 0$. Consider the (unnormalized) variational state

$$\psi^\eta_{\mathbf{k},A}(\mathbf{r}) = \frac{\sigma(z + i\tilde{B}k)}{\sigma(z)} e^{\frac{i}{2}z\bar{k}} f_\eta(\mathbf{r}) e^{-\alpha V(\mathbf{r})}, \qquad (6)$$

whose Bloch periodic part $u^\eta_{\mathbf{k},A} = e^{-i\mathbf{k}\cdot\mathbf{r}}\psi^\eta_{\mathbf{k},A}$ is a holomorphic function of $k$, meaning that this ansatz satisfies the ideal band condition. Thus, the deviation of the real wave function from the ansatz provides a measure for the violation of the ideal band condition. This deviation, measured by $\sqrt{1 - |\langle\psi_{\mathbf{k},A}|\psi^\eta_{\mathbf{k},A}\rangle|}$ [104] is plotted in Fig. 2(c) for different values of $\eta$. The deviation decreases with $\alpha$, as expected, and is of order $\sim 1\%$, indicating very small violation of the trace condition $\mathrm{Tr}g - |\Omega|$ [see Figs. 2(d) and 2(e)]. The trace violation is further reduced when $\beta$ is tuned to give the minimal bandwidth (see SM [91]). We note that the wave function [Eq. (6)], up to a $\mathbf{k}$-independent phase, corresponds to the lowest Landau level of a Dirac particle in an inhomogeneous magnetic field $\mathcal{B}(\mathbf{r}) = -\nabla^2 \log|f_\eta(\mathbf{r})e^{-\alpha V(\mathbf{r})}/\sigma(z)|$ that has a *nonzero* average flux of $2\pi$ per unit cell [8].

The wave function of the B sublattice is topologically trivial and Wannierizable. It is strongly peaked at $\mathbf{r} = 0$ and thus admits the ansatz [105] $\psi_{\mathbf{k},B}(\mathbf{r}) = \sum_\mathbf{R} e^{i\mathbf{k}\cdot\mathbf{R}} e^{\alpha V(\mathbf{r}-\mathbf{R})}$. Combined with the ansatz for the sublattice A wave function, Eq. (6), we see that projecting the $\beta = 0$ Hamiltonian onto the two flat bands yields exponentially small dispersion; the Hamiltonian only contains sublattice off-diagonal terms with the overlaps $\langle\psi_A|\psi_B\rangle \sim e^{-\alpha}$. This also explains why the value of the scalar potential $\beta$ needed to flatten the band decreases exponentially with $\alpha$ [cf. the inset in Fig. 1(e)]. A detailed analysis of the band energetics is provided in the SM [91].

*Interacting phases for the partially filled Chern band.*— Next we consider the effect of interactions on the partially filled flat Chern band. Because of valley and spin, we consider the filling $\nu \in [-4, 0]$. Using a screened Coulomb interaction $V_\mathbf{q} = (e^2/2\epsilon\epsilon_0|\mathbf{q}|)\tanh|\mathbf{q}|d$, we consider the Hamiltonian $\mathcal{H} + \mathcal{H}_\mathrm{int}$ with [9,92]

$$\mathcal{H}_\mathrm{int} = \frac{1}{2A}\sum_\mathbf{q}V_\mathbf{q}\delta\rho_\mathbf{q}\delta\rho_{-\mathbf{q}}, \qquad \rho_\mathbf{q} = \sum_{\alpha,\mathbf{k}}\lambda_{\alpha,\mathbf{q}}(\mathbf{k})c^\dagger_{\alpha,\mathbf{k}}c_{\alpha,\mathbf{k}+\mathbf{q}}, \qquad (7)$$

where $\delta\rho_\mathbf{q} = \rho_\mathbf{q} - \sum_{\alpha,\mathbf{G},\mathbf{k}}\delta_{\mathbf{q},\mathbf{G}}\lambda_{\alpha,\mathbf{G}}(\mathbf{k})$, $\alpha = (s,\tau)$ is a combined index for spin $s$ and valley $\tau$, $\mathbf{G}$ are reciprocal lattice vectors, and $\lambda_{\alpha,\mathbf{q}}(\mathbf{k}) = \langle u_{\alpha,\mathbf{k}}|u_{\alpha,\mathbf{k}+\mathbf{q}}\rangle$.

In the limit of small bandwidth, we can employ strong coupling analysis similar to TBG [9,92,93,106] to find that the ground states at integer fillings are generalized spin-valley ferromagnets. The argument is explained in detail in SM [91] and summarized here. Our setup is simpler than TBG, where there are two flat bands per flavor, and simpler than other moiré systems like twisted double bilayer graphene, where dispersion is non-negligible [56]. At $\nu = -1$ and $\nu = -3$, the ground state is a QAH spin and valley polarized insulator with Chern number $\pm 1$ that spontaneously breaks both SU(2) spin and time-reversal $\mathcal{T}$. At $\nu = -2$, we have two degenerate ground state manifolds: (i) a QAH valley ferromagnet with $C = \pm 2$ and (ii) a family of spin-polarized states with $C = 0$ consisting of a spin ferromagnet in each valley. The two manifolds (i) and (ii) are degenerate in our model, but adding an intervalley Hund's coupling lifts the degeneracy and select states in (ii) [56,91,94].

In contrast to TBG, there are no further anisotropies. In addition, intervalley coherent orders are disfavored since they involve coherent superposition of states from opposite Chern bands, leading to nodal order parameters [56,95].
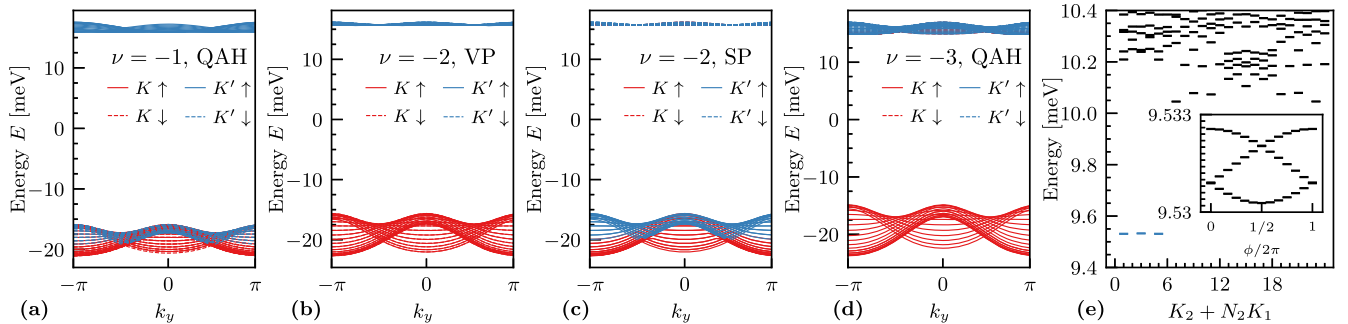


FIG. 3. (a)–(d) Self-consistent HF spectra of the strongly correlated insulators discussed in the text. System size $24 \times 24$. (e) ED spectrum at $\nu = -2/3$ on 24 $k$ points of the QAH band at $\nu = -1$, as discussed in the text. The ground state is approximately threefold degenerate (colored in blue). The inset shows the spectral flow of the three ground states under flux insertion, indicating a Laughlin state. Parameters: $\alpha = 0.4$, $\beta = 0.068$, and $E_0 = 0.325$ eV [108].

Furthermore, the interaction-generated dispersion due to Hartree-Fock corrections [13–15,106] is smaller compared to TBG with similar interaction parameters [91]. This follows from the delocalization of the $A$-sublattice wave functions across two different points, related by $M_x \mathcal{T}$ [see Fig. 2(a)], which leads to a much milder Hartree potential than that of the AA-site-localized TBG electrons. This makes the QAH more energetically favored against competing states compared to TBG [107]. The ground states at different fillings are confirmed through self-consistent HF, shown in Fig. 3. We notice here the relatively large gaps and small quasiparticle dispersion (see SM [91] for comparison with TBG).

We expect the flat ideal Chern bands to host FCIs when fractionally filled. We verify this in the simplest case where we electron-dope the $\nu = -1$ spin and valley polarized QAH state, such that the doped charge enters in a single flavor. Performing single-flavor ED at $\nu = -2/3$ shown in Fig. 3, we see clear signatures of a Laughlin state with threefold ground state degeneracy and spectral flow indicating topological order (results for a large parameter space can be found in SM [91]). Here, we have not included the interaction-generated dispersion that makes ED extremely sensitive to grid choice. However, we note the results of Ref. [19], which showed that FCIs in chiral TBG are stable up to relatively large values of dispersion. Given the smaller interaction-generated dispersion in our system [91], we expect the FCIs to survive its addition. We leave a detailed analysis of this effect to future works.

*Discussion.*—We studied a system of monolayer graphene with periodic, $C_2$-breaking PMF combined with a periodic scalar field with the same period $L_M \gg a$. This can be realized experimentally by placing graphene on top of a $C_2$-breaking substrate such as $NbSe_2$, which causes both a strain-induced $C_2$-breaking PMF and height modulation, giving a periodic potential in perpendicular electric field. Other realizations involve a network of nanorods [80] arranged in a $C_2$-breaking pattern [82], combined with a periodic scalar potential generated by a patterned dielectric [109,110] or a separate moiré hBN potential [111]. We have shown that this system hosts almost ideal topological bands whose bandwidth can be made very small by tuning the scalar potential. This establishes this system as a promising platform to study correlated topological phases such as QAH states and FCIs, which we have numerically verified. One further advantage of this system is the ability to access both a topological band and a trivial band within the same system by switching the sign of the scalar field or the gate voltage. From an experimental viewpoint, the main technical challenge in the setup based on $NbSe_2$ substrate lies in the difficulty of gating the sample since the substrate is metallic. By overcoming this technical difficulty or using a different $C_2$-breaking but insulating substrate, we predict this system to be an ideal platform to study strong correlation effects in topological bands with several advantages over twisted multilayer graphene-based moiré systems.

[1] Yuan Cao, Valla Fatemi, Ahmet Demir, Shiang Fang, Spencer L. Tomarken, Jason Y. Luo, Javier D. Sanchez-Yamagishi, Kenji Watanabe, Takashi Taniguchi, Efthimios Kaxiras, Ray C. Ashoori, and Pablo Jarillo-Herrero, Correlated insulator behaviour at half-filling in magic-angle graphene superlattices, Nature (London) **556**, 80 (2018).

[2] Matthew Yankowitz, Shaowen Chen, Hryhoriy Polshyn, Yuxuan Zhang, K. Watanabe, T. Taniguchi, David Graf, Andrea F. Young, and Cory R. Dean, Tuning superconductivity in twisted bilayer graphene, Science **363**, 1059 (2019).

[3] Xiaobo Lu, Petr Stepanov, Wei Yang, Ming Xie, Mohammed Ali Aamir, Ipsita Das, Carles Urgell, Kenji Watanabe, Takashi Taniguchi, Guangyu Zhang, Adrian Bachtold, Allan H. MacDonald, and Dmitri K. Efetov, Superconductors, orbital magnets and correlated states in magic-angle bilayer graphene, Nature (London) **574**, 653 (2019).

[4] Petr Stepanov, Ipsita Das, Xiaobo Lu, Ali Fahimniya, Kenji Watanabe, Takashi Taniguchi, Frank H. L. Koppens, Johannes Lischner, Leonid Levitov, and Dmitri K. Efetov, Untying the insulating and superconducting orders in magic-angle graphene, Nature (London) **583**, 375 (2020).

[5] Yuan Cao, Daniel Rodan-Legrain, Jeong Min Park, Noah F. Q. Yuan, Kenji Watanabe, Takashi Taniguchi, Rafael M. Fernandes, Liang Fu, and Pablo Jarillo-Herrero, Nematicity and competing orders in superconducting magic-angle graphene, Science **372**, 264 (2021).

[6] Xiaoxue Liu, Zhi Wang, K. Watanabe, T. Taniguchi, Oskar Vafek, and J. I. A. Li, Tuning electron correlation in magic-angle twisted bilayer graphene using coulomb screening, Science **371**, 1261 (2021).

[7] Fengcheng Wu and Sankar Das Sarma, Collective Excitations of Quantum Anomalous Hall Ferromagnets in Twisted Bilayer Graphene, Phys. Rev. Lett. **124**, 046403 (2020).

[8] Patrick J. Ledwith, Grigory Tarnopolsky, Eslam Khalaf, and Ashvin Vishwanath, Fractional Chern insulator states in twisted bilayer graphene: An analytical approach, Phys. Rev. Res. **2**, 023237 (2020).

[9] Patrick J. Ledwith, Eslam Khalaf, and Ashvin Vishwanath, Strong coupling theory of magic-angle graphene: A pedagogical introduction, Ann. Phys. (Amsterdam) **435**, 168646 (2021).

[10] Eslam Khalaf, Nick Bultinck, Ashvin Vishwanath, and Michael P. Zaletel, Soft modes in magic angle twisted bilayer graphene, arXiv:2009.14827.

[11] Jie Wang, Jennifer Cano, Andrew J. Millis, Zhao Liu, and Bo Yang, Exact Landau Level Description of Geometry and Interaction in a Flatband, Phys. Rev. Lett. **127**, 246403 (2021).

[12] Ahmed Abouelkomsan, Kang Yang, and Emil J. Bergholtz, Quantum metric induced phases in Moiré materials, arXiv:2202.10467.

[13] Cécile Repellin, Zhihuan Dong, Ya-Hui Zhang, and T. Senthil, Ferromagnetism in Narrow Bands of Moiré Superlattices, Phys. Rev. Lett. **124**, 187601 (2020).

[14] B. Andrei Bernevig, Biao Lian, Aditya Cowsik, Fang Xie, Nicolas Regnault, and Zhi-Da Song, Twisted bilayer graphene. V. Exact analytic many-body excitations in coulomb hamiltonians: Charge gap, goldstone modes, and absence of cooper pairing, Phys. Rev. B **103**, 205415 (2021).

[15] Jian Kang, B. Andrei Bernevig, and Oskar Vafek, Cascades between Light and Heavy Fermions in the Normal State of Magic-Angle Twisted Bilayer Graphene, Phys. Rev. Lett. **127**, 266402 (2021).

[16] Cécile Repellin and T. Senthil, Chern bands of twisted bilayer graphene: Fractional Chern insulators and spin phase transition, Phys. Rev. Res. **2**, 023238 (2020).

[17] Ahmed Abouelkomsan, Zhao Liu, and Emil J. Bergholtz, Particle-Hole Duality, Emergent Fermi Liquids, and Fractional Chern Insulators in Moiré Flatbands, Phys. Rev. Lett. **124**, 106803 (2020).

[18] Patrick Wilhelm, Thomas C. Lang, and Andreas M. Läuchli, Interplay of fractional Chern insulator and charge density wave phases in twisted bilayer graphene, Phys. Rev. B **103**, 125406 (2021).

[19] Daniel Parker, Patrick Ledwith, Eslam Khalaf, Tomohiro Soejima, Johannes Hauschild, Yonglong Xie, Andrew Pierce, Michael P. Zaletel, Amir Yacoby, and Ashvin Vishwanath, Field-tuned and zero-field fractional chern insulators in magic angle graphene, arXiv:2112.13837.

[20] Eslam Khalaf and Ashvin Vishwanath, From electrons to baby skyrmions in chern ferromagnets: A topological mechanism for spin-polaron formation in twisted bilayer graphene, arXiv:2112.06935.

[21] Yves H. Kwan, Glenn Wagner, Nick Bultinck, Steven H. Simon, and S. A. Parameswaran, Skyrmions in Twisted Bilayer Graphene: Stability, Pairing, and Crystallization, Phys. Rev. X **12**, 031020 (2022).

[22] Frank Schindler, Oskar Vafek, and B. Andrei Bernevig, Trions in twisted bilayer graphene, Phys. Rev. B **105**, 155135 (2022).

[23] Grigory Tarnopolsky, Alex Jura Kruchkov, and Ashvin Vishwanath, Origin of Magic Angles in Twisted Bilayer Graphene, Phys. Rev. Lett. **122**, 106405 (2019).

[24] Patrick J. Ledwith, Ashvin Vishwanath, and Daniel E. Parker, Vortexability: A unifying criterion for ideal fractional chern insulators, arXiv:2209.15023.

[25] Junkai Dong, Jie Wang, and Liang Fu, Dirac electron under periodic magnetic field: Platform for fractional chern insulator and generalized wigner crystal, arXiv:2208.10516.

[26] Yonglong Xie, Andrew T. Pierce, Jeong Min Park, Daniel E. Parker, Eslam Khalaf, Patrick Ledwith, Yuan Cao, Seung Hwan Lee, Shaowen Chen, Patrick R. Forrester, Kenji Watanabe, Takashi Taniguchi, Ashvin Vishwanath, Pablo Jarillo-Herrero, and Amir Yacoby, Fractional Chern insulators in magic-angle twisted bilayer graphene, Nature (London) **600**, 439 (2021).

[27] Eslam Khalaf, Shubhayu Chatterjee, Nick Bultinck, Michael P. Zaletel, and Ashvin Vishwanath, Charged skyrmions and topological origin of superconductivity in magic-angle graphene, Sci. Adv. **7**, abf5299 (2021).

[28] Shubhayu Chatterjee, Matteo Ippoliti, and Michael P. Zaletel, Skyrmion Superconductivity: DMRG evidence for a topological route to superconductivity, Phys. Rev. B **106**, 035421 (2022).

[29] Nguyen N. T. Nam and Mikito Koshino, Lattice relaxation and energy band modulation in twisted bilayer graphene, Phys. Rev. B **96**, 075311 (2017).

[30] Stephen Carr, Daniel Massatt, Steven B. Torrisi, Paul Cazeaux, Mitchell Luskin, and Efthimios Kaxiras, Relaxation and domain formation in incommensurate two-dimensional heterostructures, Phys. Rev. B **98**, 224102 (2018).

[31] Patrick J Ledwith, Eslam Khalaf, Ziyan Zhu, Stephen Carr, Efthimios Kaxiras, and Ashvin Vishwanath, Tb or not tb? Contrasting properties of twisted bilayer graphene and the alternating twist $n$-layer structures $(n = 3, 4, 5, …)$, arXiv:2111.11060.

[32] Eslam Khalaf, Alex J. Kruchkov, Grigory Tarnopolsky, and Ashvin Vishwanath, Magic angle hierarchy in twisted graphene multilayers, Phys. Rev. B **100**, 085109 (2019).

[33] Zeyu Hao, A. M. Zimmerman, Patrick Ledwith, Eslam Khalaf, Danial Haie Najafabadi, Kenji Watanabe, Takashi Taniguchi, Ashvin Vishwanath, and Philip Kim, Electric field-tunable superconductivity in alternating-twist magic-angle trilayer graphene, Science **371**, 1133 (2021).

[34] Jeong Min Park, Yuan Cao, Kenji Watanabe, Takashi Taniguchi, and Pablo Jarillo-Herrero, Tunable strongly coupled superconductivity in magic-angle twisted trilayer graphene, Nature (London) **590**, 249 (2021).

[35] Jeong Min Park, Yuan Cao, Li-Qiao Xia, Shuwen Sun, Kenji Watanabe, Takashi Taniguchi, and Pablo Jarillo-Herrero, Robust superconductivity in magic-angle multilayer graphene family, Nat. Mater. **21**, 877 (2022).

[36] Yiran Zhang, Robert Polski, Cyprian Lewandowski, Alex Thomson, Yang Peng, Youngjoon Choi, Hyunjin Kim, Kenji Watanabe, Takashi Taniguchi, Jason Alicea *et al.*, Promotion of superconductivity in magic-angle graphene multilayers, Science **377**, 1538 (2022).

[37] Shaowen Chen, Minhao He, Ya-Hui Zhang, Valerie Hsieh, Zaiyao Fei, K. Watanabe, T. Taniguchi, David H. Cobden, Xiaodong Xu, Cory R. Dean, and Matthew Yankowitz, Electrically tunable correlated and topological states in twisted monolayer–bilayer graphene, Nat. Phys. **17**, 374 (2021).

[38] Minhao He, Ya-Hui Zhang, Yuhao Li, Zaiyao Fei, Kenji Watanabe, Takashi Taniguchi, Xiaodong Xu, and Matthew Yankowitz, Competing correlated states and abundant orbital magnetism in twisted monolayer-bilayer graphene, Nat. Commun. **12**, 4727 (2021).

[39] H. Polshyn, Y. Zhang, M. A. Kumar, T. Soejima, P. Ledwith, K. Watanabe, T. Taniguchi, A. Vishwanath, M. P. Zaletel, and A. F. Young, Topological charge density waves at half-integer filling of a moiré superlattice, Nat. Phys. **18**, 42 (2021).

[40] E. Suárez Morell, M. Pacheco, L. Chico, and L. Brey, Electronic properties of twisted trilayer graphene, Phys. Rev. B **87**, 125414 (2013).

[41] H. Polshyn, J. Zhu, M. A. Kumar, Y. Zhang, F. Yang, C. L. Tschirhart, M. Serlin, K. Watanabe, T. Taniguchi, A. H. MacDonald, and A. F. Young, Electrical switching of magnetic order in an orbital Chern insulator, Nature (London) **588**, 66 (2020).

[42] Si-yu Li, Zhengwen Wang, Yucheng Xue, Yingbo Wang, Shihao Zhang, Jianpeng Liu, Zheng Zhu, Kenji Watanabe, Takashi Taniguchi, Hong-jun Gao *et al.*, Imaging topological and correlated insulating states in twisted mono-layer-bilayer graphene, Nat. Commun. **13**, 1 (2022).

[43] Ling-Hui Tong, Qingjun Tong, Li-Zhen Yang, Yue-Ying Zhou, Qilong Wu, Yuan Tian, Li Zhang, Lijie Zhang, Zhihui Qin, and Long-Jing Yin, Spectroscopic Visualization of Flat Bands in Magic-Angle Twisted Monolayer-Bilayer Graphene: Coexistence of Localization and Delocalization, Phys. Rev. Lett. **128**, 126401 (2022).

[44] Xiaomeng Liu, Zeyu Hao, Eslam Khalaf, Jong Yeon Lee, Yuval Ronen, Hyobin Yoo, Danial Haei Najafabadi, Kenji Watanabe, Takashi Taniguchi, Ashvin Vishwanath, and Philip Kim, Tunable spin-polarized correlated states in twisted double bilayer graphene, Nature (London) **583**, 221 (2020).

[45] Yuan Cao, Daniel Rodan-Legrain, Oriol Rubies-Bigorda, Jeong Min Park, Kenji Watanabe, Takashi Taniguchi, and Pablo Jarillo-Herrero, Tunable correlated states and spin-polarized phases in twisted bilayer–bilayer graphene, Nature (London) **583**, 215 (2020).

[46] Minhao He, Yuhao Li, Jiaqi Cai, Yang Liu, K. Watanabe, Takashi Taniguchi, Xiaodong Xu, and Matthew Yankowitz, Symmetry breaking in twisted double bilayer graphene, Nat. Phys. **17**, 1 (2021).

[47] Ya-Hui Zhang, Dan Mao, Yuan Cao, Pablo Jarillo-Herrero, and T. Senthil, Nearly flat chern bands in moiré super-lattices, Phys. Rev. B **99**, 075127 (2019).

[48] Jong Yeon Lee, Eslam Khalaf, Shang Liu, Xiaomeng Liu, Zeyu Hao, Philip Kim, and Ashvin Vishwanath, Theory of correlated insulating behaviour and spin-triplet super-conductivity in twisted double bilayer graphene, Nat. Commun. **10**, 5333 (2019).

[49] Minhao He, Yuhao Li, Jiaqi Cai, Yang Liu, K. Watanabe, T. Taniguchi, Xiaodong Xu, and Matthew Yankowitz, Symmetry breaking in twisted double bilayer graphene, Nat. Phys. **17**, 26 (2020).

[50] Minhao He, Jiaqi Cai, Ya-Hui Zhang, Yang Liu, Yuhao Li, Takashi Taniguchi, Kenji Watanabe, David H. Cobden, Matthew Yankowitz, and Xiaodong Xu, Chirality-dependent topological states in twisted double bilayer graphene, arXiv:2109.08255.

[51] Le Liu, Shihao Zhang, Yanbang Chu, Cheng Shen, Yuan Huang, Yalong Yuan, Jinpeng Tian, Jian Tang, Yiru Ji, Rong Yang, Kenji Watanabe, Takashi Taniguchi, Dongxia Shi, Jianpeng Liu, Wei Yang, and Guangyu Zhang, Isospin

competitions and valley polarized correlated insulators in twisted double bilayer graphene, Nat. Commun. **13**, 3292 (2022).

[52] Patrick J. Ledwith, Ashvin Vishwanath, and Eslam Khalaf, Family of Ideal Chern Flatbands with Arbitrary Chern Number in Chiral Twisted Graphene Multilayers, Phys. Rev. Lett. **128**, 176404 (2022).

[53] Jie Wang and Zhao Liu, Hierarchy of Ideal Flatbands in Chiral Twisted Multilayer Graphene Models, Phys. Rev. Lett. **128**, 176403 (2022).

[54] Junkai Dong, Patrick J. Ledwith, Eslam Khalaf, Jong Yeon Lee, and Ashvin Vishwanath, Exact many-body ground states from decomposition of ideal higher chern bands: Applications to chirally twisted graphene multilayers, arXiv:2210.13477.

[55] Jie Wang, Semyon Klevtsov, and Zhao Liu, Origin of model fractional chern insulators in all topological ideal flatbands: Explicit color-entangled wavefunction and exact density algebra, Phys. Rev. Res. **5**, 023167 2023.

[56] Jong Yeon Lee, Eslam Khalaf, Shang Liu, Xiaomeng Liu, Zeyu Hao, Philip Kim, and Ashvin Vishwanath, Theory of correlated insulating behaviour and spin-triplet super-conductivity in twisted double bilayer graphene, Nat. Commun. **10**, 5333 (2019).

[57] We note also other non-moiré alternatives to TBG [58,59], which capture some aspects of the moiré physics and show promising tunablities.

[58] Tymoteusz Salamon, Alessio Celi, Ravindra W. Chhajlany, Irénée Frérot, Maciej Lewenstein, Leticia Tarruell, and Debraj Rakshit, Simulating Twistronics without a Twist, Phys. Rev. Lett. **125**, 030504 (2020).

[59] Constantinos Valagiannopoulos, Electromagnetic Analog to Magic Angles in Twisted Bilayers of Two-Dimensional Media, Phys. Rev. Appl. **18**, 044011 (2022).

[60] Pouyan Ghaemi, Jérôme Cayssol, Donna N. Sheng, and Ashvin Vishwanath, Fractional Topological Phases and Broken Time-Reversal Symmetry in Strained Graphene, Phys. Rev. Lett. **108**, 266801 (2012).

[61] Zhen Bi, Noah F. Q. Yuan, and Liang Fu, Designing flat bands by strain, Phys. Rev. B **100**, 035448 (2019).

[62] Alexander Lau, Timo Hyart, Carmine Autieri, Anffany Chen, and Dmitry I. Pikulin, Designing Three-Dimensional Flat Bands in Nodal-Line Semimetals, Phys. Rev. X **11**, 031017 (2021).

[63] Li-Zhen Yang, Ling-Hui Tong, Cheng-Sheng Liao, Qilong Wu, Xiaoshuai Fu, Yue-Ying Zhou, Yuan Tian, Li Zhang, Lijie Zhang, Meng-Qiu Cai *et al.*, Origami-controlled strain engineering of tunable flat bands and correlated states in folded graphene, Phys. Rev. Mater. **6**, L041001 (2022).

[64] Evelyn Tang and Liang Fu, Strain-induced partially flat band, helical snake states and interface superconductivity in topological crystalline insulators, Nat. Phys. **10**, 964 (2014).

[65] Hidekatsu Suzuura and Tsuneya Ando, Phonons and electron-phonon scattering in carbon nanotubes, Phys. Rev. B **65**, 235412 (2002).

[66] Juan L. Manes, Symmetry-based approach to electron-phonon interactions in graphene, Phys. Rev. B **76**, 045430 (2007).

[67] Eun-Ah Kim and A. H. Castro Neto, Graphene as an electronic membrane, Europhys. Lett. **84**, 57007 (2008).

[68] F. Guinea, Baruch Horovitz, and P. Le Doussal, Gauge field induced by ripples in graphene, Phys. Rev. B **77**, 205421 (2008).

[69] Vitor M. Pereira and A. H. Castro Neto, Strain Engineering of Graphene's Electronic Structure, Phys. Rev. Lett. **103**, 046801 (2009).

[70] Maria A. H. Vozmediano, M. I. Katsnelson, and Francisco Guinea, Gauge fields in graphene, Phys. Rep. **496**, 109 (2010).

[71] T. Low, F. Guinea, and M. I. Katsnelson, Gaps tunable by electrostatic gates in strained graphene, Phys. Rev. B **83**, 195436 (2011).

[72] Fernando de Juan, Mauricio Sturla, and Maria A. H. Vozmediano, Space Dependent Fermi Velocity in Strained Graphene, Phys. Rev. Lett. **108**, 227205 (2012).

[73] Juan L. Mañes, Fernando de Juan, Mauricio Sturla, and María A. H. Vozmediano, Generalized effective Hamiltonian for graphene under nonuniform strain, Phys. Rev. B **88**, 155405 (2013).

[74] Fernando de Juan, Juan L. Manes, and María A. H. Vozmediano, Gauge fields from strain in graphene, Phys. Rev. B **87**, 165131 (2013).

[75] Francisco Guinea, M. I. Katsnelson, and A. K. Geim, Energy gaps and a zero-field quantum hall effect in graphene by strain engineering, Nat. Phys. **6**, 30 (2010).

[76] Tony Low and F. Guinea, Strain-induced pseudomagnetic field for novel graphene electronics, Nano Lett. **10**, 3551 (2010).

[77] Since the vector potential scales as the derivative of the displacement $u$, a uniform field requires a quadratic dependence of $u$ on distance [75,76].

[78] N. Levy, S. A. Burke, K. L. Meaker, M. Panlasigui, A. Zettl, F. Guinea, A. H. Castro Neto, and Michael F. Crommie, Strain-induced pseudo–magnetic fields greater than 300 tesla in graphene nanobubbles, Science **329**, 544 (2010).

[79] Si-Yu Li, Ying Su, Ya-Ning Ren, and Lin He, Valley Polarization and Inversion in Strained Graphene via Pseudo-Landau Levels, Valley Splitting of Real Landau Levels, and Confined States, Phys. Rev. Lett. **124**, 106802 (2020).

[80] Yuhang Jiang, Jinhai Mao, Junxi Duan, Xinyuan Lai, Kenji Watanabe, Takashi Taniguchi, and Eva Y. Andrei, Visualizing strain-induced pseudomagnetic fields in graphene through an hbn magnifying glass, Nano Lett. **17**, 2839 (2017).

[81] Jinhai Mao, Slaviša P. Milovanović, Miša Anđelković, Xinyuan Lai, Yang Cao, Kenji Watanabe, Takashi Taniguchi, Lucian Covaci, Francois M. Peeters, Andre K. Geim *et al.*, Evidence of flat bands and correlated states in buckled graphene superlattices, Nature (London) **584**, 215 (2020).

[82] Võ Tiến Phong and Eugene J. Mele, Boundary Modes from Periodic Magnetic and Pseudomagnetic Fields in Graphene, Phys. Rev. Lett. **128**, 176406 (2022).

[83] Christophe De Beule, Vo Tien Phong, and E. J. Mele, Network model for periodically strained graphene, arXiv:2209.02554.

[84] S. P. Milovanović, M. Anđelković, L. Covaci, and F. M. Peeters, Band flattening in buckled monolayer graphene, Phys. Rev. B **102**, 245427 (2020).

[85] Antonio L. R. Manesco, Jose L. Lado, Eduardo V. S. Ribeiro, Gabrielle Weber, and Durval Rodrigues Jr, Correlations in the elastic landau level of spontaneously buckled graphene, 2D Mater. **8**, 015011 (2020).

[86] Antonio L. R. Manesco and Jose L. Lado, Correlation-induced valley topology in buckled graphene superlattices, 2D Mater. **8**, 035057 (2021).

[87] Yarden Sheffer, Raquel Queiroz, and Ady Stern, Symmetries as the guiding principle for flattening bands of dirac fermions, arXiv:2205.02784.

[88] P. San-Jose, J. González, and F. Guinea, Non-Abelian Gauge Potentials in Graphene Bilayers, Phys. Rev. Lett. **108**, 216802 (2012).

[89] It is worth noting that under the time-reversal symmetry $\mathcal{T}$, the other valley will have an opposite Chern number and a reversed pseudomagnetic field that defers from a real magnetic field. Apart from the change of the signs, the analysis made for the valley in the main text can be readily applied to the other. However, when including the interaction, the time-reversal symmetry is likely broken, and we have to consider two valleys together that is discussed in the strong coupling analysis.

[90] We note that although a $\sigma_z$ term is symmetry-allowed, its effect on the two bands close to neutrality can be absorbed into the scalar potential that provides an approximately constant $\sigma_z$ term [91].

[91] See Supplemental Material at http://link.aps.org/supplemental/10.1103/PhysRevLett.131.096401 for more details, which includes Refs. [9,13,14,16,26,92–97].

[92] Nick Bultinck, Eslam Khalaf, Shang Liu, Shubhayu Chatterjee, Ashvin Vishwanath, and Michael P. Zaletel, Ground State and Hidden Symmetry of Magic-Angle Graphene at Even Integer Filling, Phys. Rev. X **10**, 031034 (2020).

[93] Biao Lian, Zhi-Da Song, Nicolas Regnault, Dmitri K. Efetov, Ali Yazdani, and B. Andrei Bernevig, Twisted bilayer graphene. IV. Exact insulator ground states and phase diagram, Phys. Rev. B **103**, 205414 (2021).

[94] Ya-Hui Zhang, Dan Mao, Yuan Cao, Pablo Jarillo-Herrero, and T. Senthil, Nearly flat chern bands in moiré superlattices, Phys. Rev. B **99**, 075127 (2019).

[95] Nick Bultinck, Shubhayu Chatterjee, and Michael P. Zaletel, Mechanism for Anomalous Hall Ferromagnetism in Twisted Bilayer Graphene, Phys. Rev. Lett. **124**, 166601 (2020).

[96] Aaron L. Sharpe, Eli J. Fox, Arthur W. Barnard, Joe Finney, Kenji Watanabe, Takashi Taniguchi, M. A. Kastner, and David Goldhaber-Gordon, Emergent ferromagnetism near three-quarters filling in twisted bilayer graphene, Science **365**, 605 (2019).

[97] M. Serlin, C. L. Tschirhart, H. Polshyn, Y. Zhang, J. Zhu, K. Watanabe, T. Taniguchi, L. Balents, and A. F. Young, Intrinsic quantized anomalous Hall effect in a moiré heterostructure, Science **367**, 900 (2019).

[98] For the purpose of this Letter, we require $L_M$ to be sufficiently large compared to the lattice constant to ignore higher-order correction, but we also require the

dimensionless parameter $\alpha$, which scales as $L_M^2$, to not be very large so that we can obtain a well-isolated band, whose gap from the other bands exceeds the interaction scale. It is worth mentioning that for a very large $\alpha$ (namely, $L_M \gg l_{\mathcal{B}}$), all bandwidths and band gaps will get exponentially squeezed as shown in Fig. 1(e).

[99] Here, we assumed the zero is at $r = 0$ to preserve rotation symmetry.

[100] F. D. M. Haldane, A modular-invariant modified weierstrass sigma-function as a building block for lowest-landau-level wavefunctions on the torus, J. Math. Phys. (N.Y.) **59**, 071901 (2018).

[101] Bruno Mera and Tomoki Ozawa, Kähler geometry and chern insulators: Relations between topology and the quantum metric, Phys. Rev. B **104**, 045104 (2021).

[102] Tomoki Ozawa and Bruno Mera, Relations between topology and the quantum metric for chern insulators, Phys. Rev. B **104**, 045103 (2021).

[103] While the value of $\alpha$ we use, $\alpha = 0.4$ is not large, we note that in our convention, the maximum value of the potential is 6, which leads to the exponential factor $e^{-0.4 \times 6} = e^{-2.4} \approx 0.09$.

[104] Let us write the real wave function for $A$ sublattice at $\boldsymbol{k}$ as the ansatz plus a small deviation: $|\psi_{\boldsymbol{k},A}\rangle = |\psi_{\boldsymbol{k},A}^\eta\rangle + |\delta\psi_{\boldsymbol{k},A}\rangle$. If the real wave function and ansatz are both normalized, we have $\||\psi_{\boldsymbol{k},A}\rangle\|^2 = 1 = 1 + 2\text{Re}\langle\delta\psi_{\boldsymbol{k},A}|\psi_{\boldsymbol{k},A}^\eta\rangle + \||\delta\psi_{\boldsymbol{k},A}\rangle\|^2$. Thus, to the first order in $|\delta\psi_{\boldsymbol{k},A}\rangle$, we have $\text{Re}\langle\delta\psi_{\boldsymbol{k},A}|\psi_{\boldsymbol{k},A}^\eta\rangle = 0$, which indicates that overlap deviation $1 - |\langle\psi_{\boldsymbol{k},A}|\psi_{\boldsymbol{k},A}^\eta\rangle|$ goes quadratic with $|\delta\psi_{\boldsymbol{k},A}\rangle$. However, the trace condition violation normally goes linearly with $|\delta\psi_{\boldsymbol{k},A}\rangle$. Thus, we plot the square root overlap deviation in Fig. 2(d) as to better compare with trace violation.

[105] The reader may wonder why a similar ansatz to that of sublattice $A$ does not work here, which would yield a $C = -1$ band antiholomorphic in $k_x + ik_y$. In fact, such an ansatz is possible but it necessarily mixes multiple (exponentially squeezed) $B$-sublattice bands. However, we expect the topologically trivial strongly localized band, that we obtain from diagonalizing the Hamiltonian, to dominate the low-energy $B$-sublattice physics because it is straightforward to keep particles apart in this band. In contrast, the $A$-sublattice bands have a more robust topology because their density is localized at two distinct points in the unit cell related by $M_x\mathcal{T}$.

[106] Jian Kang and Oskar Vafek, Strong Coupling Phases of Partially Filled Twisted Bilayer Graphene Narrow Bands, Phys. Rev. Lett. **122**, 246401 (2019).

[107] Andrew T. Pierce, Yonglong Xie, Jeong Min Park, Eslam Khalaf, Seung Hwan Lee, Yuan Cao, Daniel E. Parker, Patrick R. Forrester, Shaowen Chen, Kenji Watanabe *et al.*, Unconventional sequence of correlated chern insulators in magic-angle twisted bilayer graphene, Nat. Phys. **17**, 1210 (2021).

[108] This value corresponds to $L_M \approx 13.3$ nm that matches that of TBG at the first magic angle. This makes it easier to compare the resulting gaps and dispersion with those of TBG.

[109] Jennifer Cano, Shiang Fang, J. H. Pixley, and Justin H. Wilson, Moiré superlattice on the surface of a topological insulator, Phys. Rev. B **103**, 155157 (2021).

[110] Daniele Guerci, Jie Wang, J. H. Pixley, and Jennifer Cano, Designer meron lattice on the surface of a topological insulator, arXiv:2203.04986.

[111] Pei Zhao, Chengxin Xiao, and Wang Yao, Universal superlattice potential for 2d materials from twisted interface inside h-bn substrate, npj 2D Mater. Appl. **5**, 1 (2021).